Tethered Lipid Bilayers on Electrolessly Deposited Gold for Bioelectronic Applications

Neeraj Kohli,[†] Brian L. Hassler,[†] Lavanya Parthasarathy,[†] Rudy J. Richardson,[‡] Robert Y. Ofoli,[†] Robert M. Worden,*[,†] and Ilsoon Lee*[,†]

Department of Chemical Engineering and Materials Science, Michigan State University, East Lansing, Michigan 48824, and Toxicology Program, Department of Environmental Health Sciences, School of Public Health, The University of Michigan, Ann Arbor, Michigan 48109-2029

Received April 24, 2006; Revised Manuscript Received September 14, 2006

This paper presents the formation of a novel biomimetic interface consisting of an electrolessly deposited gold film overlaid with a tethered bilayer lipid membrane (tBLM). Self-assembly of colloidal gold particles was used to create an electrolessly deposited gold film on a glass slide. The properties of the film were characterized using field-effect scanning electron microscopy, energy dispersive spectroscopy, and atomic force microscopy. Bilayer lipid membranes were then tethered to the gold film by first depositing an inner molecular leaflet using a mixture of 1,2-dipalmitoyl-*sn*-glycero-3-phosphoethanolamine-*N*-[3-(2-pyridyldithio)propionate], 1,2-di-*O*-phytanyl-*sn*-glycero-3-phosphoethanolamine (DPGP), and cystamine in ethanol onto a freshly prepared electrolessly deposited gold surface. The outer leaflet was then formed by the fusion of liposomes made from DPGP or 1,2-dioleoyl-*sn*-glycero-3-phosphocholine on the inner leaflet. To provide functionality, two membrane biomolecules were also incorporated into the tBLMs: the ionophore valinomycin and a segment of neuropathy target esterase containing the esterase domain. Electrochemical impedance spectroscopy, UV/visible spectroscopy, and fluorescence recovery after pattern photobleaching were used to characterize the resulting biomimetic interfaces and confirm the biomolecule activity of the membrane. Microcontact printing was used to form arrays of electrolessly deposited gold patterns on glass slides. Subsequent deposition of lipids yielded arrays of tBLMs. This approach can be extended to form functional biomimetic interfaces on a wide range of inexpensive materials, including plastics. Potential applications include high-throughput screening of drugs and chemicals that interact with cell membranes and for probing, and possibly controlling, interactions between living cells and synthetic membranes. In addition, the gold electrode provides the possibility of electrochemical applications, including biocatalysis, bio-fuel cells, and biosensors.

Introduction

Living cells efficiently perform many vital sensing, signaling, catalytic, transport, and bioelectronic processes on the molecular scale. These processes typically occur in cell membranes, whose principal components include a bilayer lipid membrane (BLM) and membrane proteins. To mimic these processes in the laboratory, biomimetic interfaces consisting of supported bilayer lipid membranes (sBLMs) with embedded membrane proteins and other biomolecules have been formed on glass, silica, and metal surfaces.[1−19] Such sBLMs have enabled researchers to probe properties such as phase transition, lateral diffusion, permeation, and lipid−protein interactions.[20] However, supported membranes have two serious shortcomings: (1) there is no cushion between the surface and the sBLM to provide space for extramembrane moieties of membrane proteins or other biomolecules and to allow lateral mobility of the membrane components, and (2) unlike most cell membranes, they lack ionic reservoirs on both sides of the bilayer. Such reservoirs are needed to achieve protein- or ionophore-mediated transport across the BLM and perform certain bioelectronic applications, such as electrochemical impedance spectroscopy.

To overcome these limitations, new approaches that involve the use of hydrophilic cushions on which BLMs can be deposited are being adopted by researchers. Such cushions have consisted of polyelectrolyte multilayers (PEMs), polymer films, and polymeric tethers (e.g., poly (ethylene glycol) (PEG) tether).[21−33] The tethered BLMs (tBLMs) offer the following advantages: (1) they are robust and have high insulating ability and (2) they have a submembrane space that can serve as an ionic reservoir as well as provide adequate space for incorporated membrane proteins. However, these tBLM systems have primarily been used for sensor applications and have not been applied in areas such as biocatalysis and biofuel cells. Therefore, novel approaches that can extend the application range of tBLMs to these areas are of commercial and scientific interest.

Microcontact printing (μCP)[34] is a soft lithographic technique used in physics, chemistry, materials science, and biology to transfer patterned, thin, organic films to surfaces, with submicron resolution. Unlike other fabrication methods that merely provide topographic contrast between the feature and the background, μCP also allows chemical contrast to be achieved via selection of an appropriate ink. μCP offers advantages over conventional photolithographic techniques, because it is simple to perform and is not diffraction-limited. This technique has been used to make patterns of various small and large molecules on metals and silicon substrates,[35−38]as well as to deposit proteins,[39] biological cells,[40−42]and polyelectrolyte aggregates. μCP has also been used to generate arrays of sBLMs on glass slides.[43−46] However, this approach has not been demonstrated using

* To whom correspondence should be addressed. Fax: (517) 432-1105. E-mail: leeil@egr.msu.edu (I.L.), worden@egr.msu.edu (R.M.W.).
[†] Michigan State University.
[‡] The University of Michigan.

10.1021/bm0603995 CCC: $33.50
Published on Web 11/08/2006

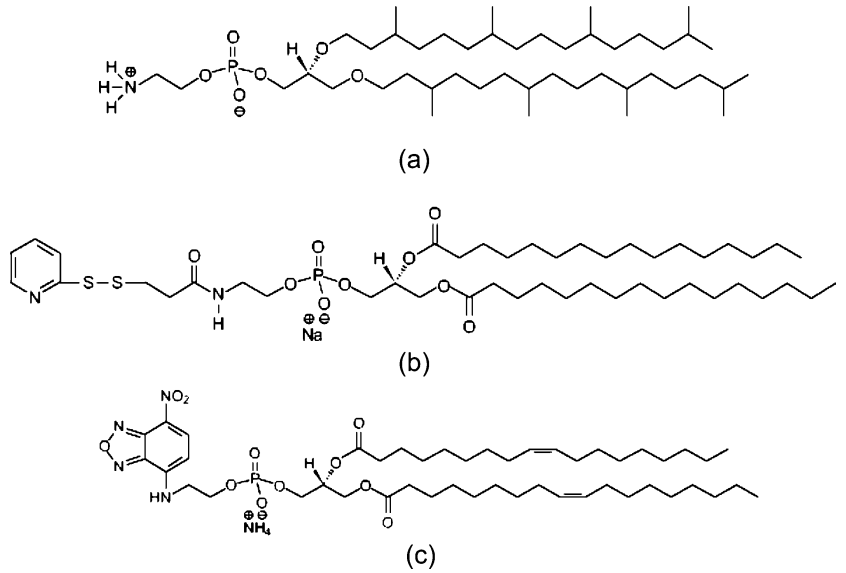

Figure 1. Structure of lipid molecules used to fabricate tBLM: (a) DPGP (mobile lipid), (b) DGP (reservoir lipid), and (c) NBD-PE.

tBLMs; thus, methods are needed with which to assemble tBLM arrays on diverse types of surfaces.

Electroless deposition is an inexpensive metal-plating technique that, unlike chemical vapor deposition (CVD) or physical vapor deposition (PVD), can easily be performed on a laboratory bench top and in aqueous solutions. It is an autocatalytic redox process in which metal cations in solution are chemically reduced and deposited on the surface.[47−56] Recently, another form of electroless deposition (self-assembly of colloidal metal particles), has also generated interest for the fabrication of metal films and nanostructures.[57,58] This approach has been used to generate thin films of gold, platinum, and silver on different substrates.

An important potential application of electroless deposition is in fabrication of functionalized electrodes or electrode arrays. Although methods such as CVD or PVD have been used in the past for making arrays, these methods are expensive and require a primer such as Ti or Cr for improved adhesion to the surface, which leads to problems such as grain boundary diffusion. In addition, nanometer scale control over properties is difficult to achieve using this approach.[58] On the other hand, electroless deposition does not require an adhesion layer, and it can be used to tune the properties of arrays or films of metals with nanometer-scale precision on virtually any surface, including glass, silicon wafers, and mechanically flexible plastics.[58] Moreover, electroless deposition is well-suited for use with porous materials, because capillary forces can draw the gold salt solution into interior pores.

This paper presents fabrication of a novel biomimetic interface consisting of a conductive, electrolessly deposited gold film overlaid with a tBLM. The properties of the gold film were characterized using field-effect scanning electron microscopy (FE-SEM), energy dispersive spectroscopy (EDS), and atomic force microscopy (AFM). The fluidity of the tBLM was measured using fluorescence recovery after pattern photobleaching (FRAPP). The suitability of the interface to maintain membrane proteins or other biomolecules in a functional conformation was shown using the ionophore valinomycin, and a segment of neuropathy target esterase (NTE) containing its catalytic domain (NEST). High-density microarrays of the biomimetic interface on glass were generated using μCP.

Experimental Section

Materials. 1,2-Dipalmitoyl-*sn*-glycero-3-phosphoethanolamine-*N*-[3-(2-pyridyldithio)propionate] (DGP, Figure 1a), 1,2-dioleoyl-*sn*-glycero-3-phosphocholine (DOPC), 1,2-di-*O*-phytanyl-*sn*-glycero-3-phosphoethanolamine (DPGP, Figure 1b), and 1,2-dioleoyl-*sn*-glycero-3-phosphoethanolamine-*N*-(7-nitro-2,1,3-benzoxadiazol-4-yl) (NBD-PE, Figure 1c) were purchased from Avanti Polar Lipids (Alabaster, AL). Cysteamine, 3-mercaptopropyltrimethoxy silane (MPS), gold chloride trihydrate ($HAuCl_4 \cdot 3H_2O$), hydroxylamine, dithiothreitol (DTT), fluorosilanes, and sodium citrate dihydrate were obtained from Sigma (St. Louis, MO). All reagents were of the highest purity grade available and were used without any further purification. Poly(ethylene glycol) (PEG)−silane 2000 (molecular weight 2176.7) was obtained from Nektar Therapeutics (San Carlos, CA). Sylgard 184 silicone elastomer kit (Dow Corning, Midland, MI) was used to prepare the poly(dimethylsiloxane) (PDMS) stamps for mCP. Deionized (DI) water (18.2 MΩ) was supplied by a Nanopure-UV four-stage purifier (Barnstead International, Dubuque, IA); the purifier was equipped with a UV source and a final 0.2 μm filter. All aqueous solutions were prepared using DI water.

Preparation of Stamps. The PDMS stamps were made by pouring a 10:1 (w/w) solution of elastomer and initiator over a pretreated silicon master, which acts as a mold, to allow the surface morphology of the stamp to form a negative replica of the master. The silicon master was pretreated with fluorosilanes to facilitate the removal of the PDMS stamps. The mixture was allowed to cure overnight at 60 °C and then peeled off. The masters were prepared in the Keck microfabrication facility at MSU and consisted of features (parallel lines and circles) from 1 to 20 μm.

Synthesis of Colloidal Gold Particles. An aqueous sodium citrate solution (106 mL, 2.2 mM) was rapidly boiled in a flask, and 1 mL of 24.3 mM $HAuCl_4 \cdot 3H_2O$ was rapidly added under vigorous stirring. The solution was boiled for 15 min, cooled to room temperature, and stored at 4 °C.[58]

Formation of Gold Film and Patterns by Electroless Deposition. The gold films were fabricated as illustrated in Figure 2 using a variation of the method reported by Fren.[58,59] Glass slides were cleaned in piranha solution [7 parts by volume concentrated H_2SO_4 and 3 parts 30% (v/v) H_2O_2] and then washed with DI water and dried under nitrogen. The slides were dipped into a 1% (v/v) solution of MPS in methanol for 10 min with stirring, rinsed with methanol, and heated to 110 °C for 2 h to complete the silanization. The surface-modified slides were then immersed in colloidal gold solution at room temperature (22 ± 1 °C) for 2 h to allow thiol bonds to form between gold nanoparticles and

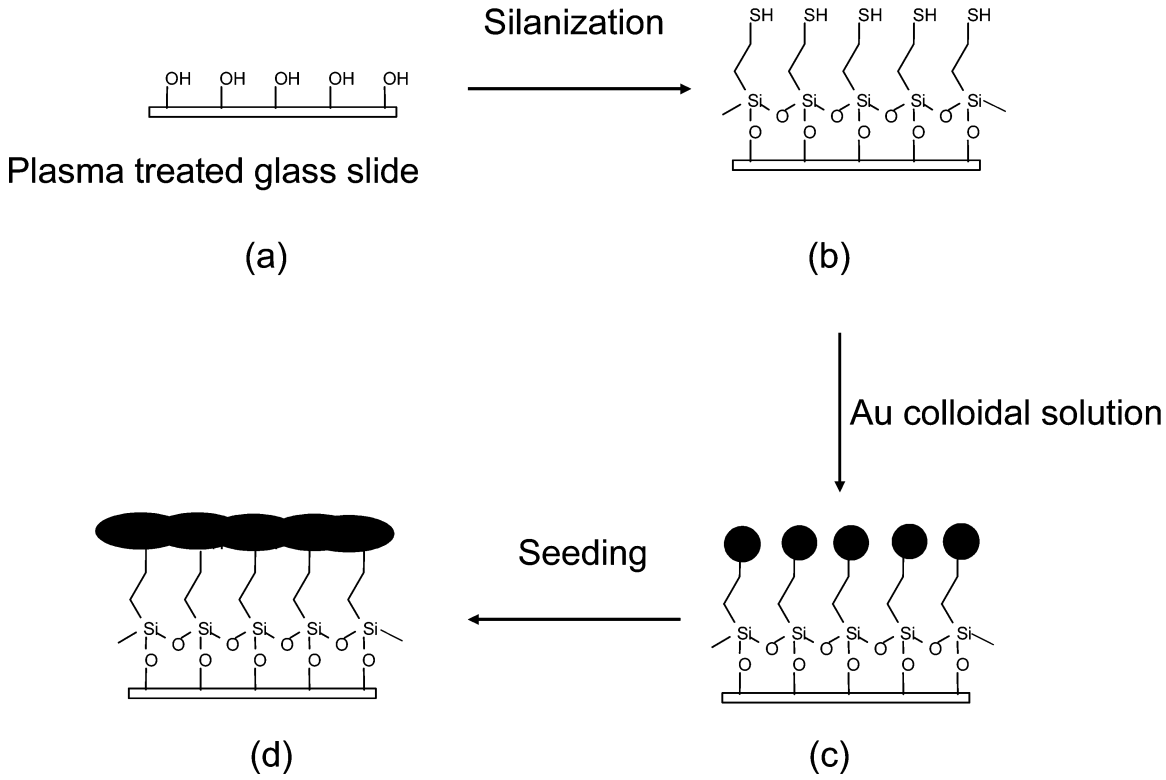

Figure 2. Schematic representation of the process for depositing Au films: (a) plasma-treated glass slide, (b) slide after silanization with MPS, (c) modified slide after dipping in Au particle solution, and (d) conductive Au film after seeding step

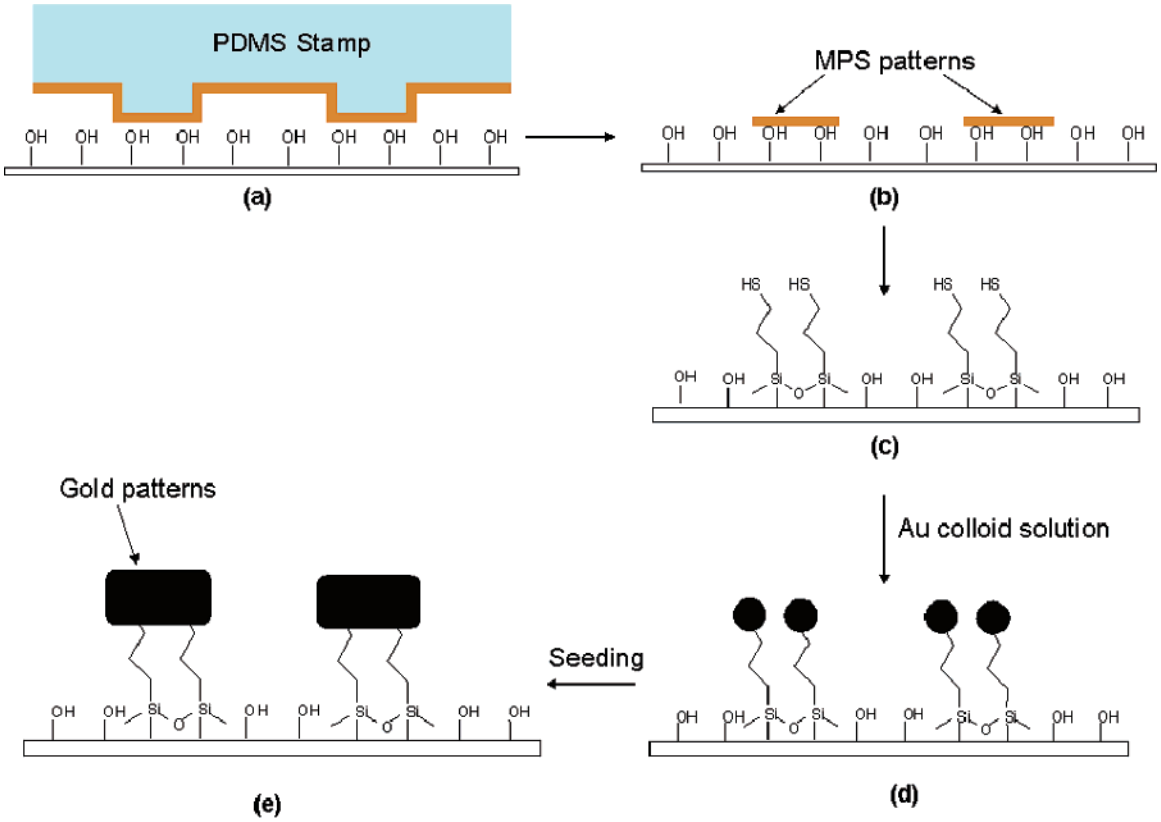

Figure 3. Schematic representation of the process for fabricating Au patterns: (a) PDMS stamping of MPS on a glass slide, (b) MPS patterns on a glass slide, (c) MPS-patterned modified glass slide after heating, (d) MPS-patterned slide after dipping in Au colloid solution, and (e) Au patterns after seeding step.

sulfur groups. The slides were then rinsed with DI water and immersed in 200 mL of aqueous solution containing 2.6 mg of hydroxylamine and 20 mg of $HAuCl_4 \cdot 3H_2O$ under constant agitation for 30 min. This step, called seeding, resulted in chemical reduction of gold ions onto the immobilized gold nanoparticles. The seeding process was repeated three times to achieve a continuous, conductive film.

To obtain gold patterns (Figure 3), a PDMS stamp was dipped into a 1 mM solution of MPS in ethanol for 5 min. The stamp was washed

with absolute ethanol, dried under nitrogen, and brought into contact with a glass slide. The stamp was removed after 2 min, and the resulting MPS patterned slide was washed with ethanol to remove loosely bound MPS. The slide was heated to 110 °C for 2 h and immersed in colloidal gold solution. The patterned slide was then sonicated in DI water for 10 min to remove loosely bound gold particles from the background of the glass slides. The gold-particle-patterned slide was then exposed to the seeding solution for 30 min three times to create gold patterns.

Preparation of Liposomes for Fluorescence and Electrochemical Measurements. For fluorescence experiments, small unilamellar liposomes (~20 ± 5 nm) were prepared by adding 20 mg of DPGP and 0.2 mg of NBD-PE in 1 mL of chloroform. This mixture was then dried under nitrogen, making sure the lipid formed a thin cakelike film on the walls of the test tube. The residual chloroform was removed under vacuum. The lipids were then reconstituted in 20 mL of 0.1 M aqueous NaCl solution, and the resulting liposome solution was sonicated with a Bransonic bath sonicator (Branson Ultrasonics Corp., Danbury, CT) until it became clear. Liposomes were prepared in the same way for electrochemical experiments, except no NBD-PE was added. The liposome size was determined using a Coulter N4 MD particle size analyzer (Coulter Electronics Inc., Hialeah, FL)

Formation of tBLMs Containing Valinomycin. The inner leaflet of the tBLM was formed by dipping a freshly prepared electrolessly deposited gold slide into an ethanolic solution of 1 mM DGP, 1 mM DPGP, and 500 μM cystamine for 2 h. The slide was washed with absolute ethanol and dried under nitrogen. The modified slide was dipped in liposome solution (1 mg/mL) for 45 min and washed with 0.1 M aqueous NaCl solution to obtain the outer leaflet.

An ethanolic stock solution of valinomycin (2 mg/mL) was diluted in the aqueous solution to obtain a valinomycin concentration of 5×10^{-7} M and allowed to equilibrate for 1 h at room temperature. No change in impedance was observed on valinomycin insertion in this aqueous solution (0.1 M NaCl). However, the impedance dropped when this solution was replaced with another solution containing 0.05 M NaCl and 0.05 M KCl, providing evidence of the insertion and activity of this potassium-selective ionophore into the tBLM.

Formation of NEST-Containing Liposomes (NEST−DOPC Liposomes). NEST was expressed and purified according to published procedures.[60] For incorporation into liposomes, NEST solution (0.1 mg/mL) in PEN buffer (50 mM phosphate buffer, 0.5 mM EDTA, and 300 mM NaCl) containing 0.3% (w/v) CHAPS was mixed with DOPC (10 mg/mL in 9%(w/v) CHAPS) in 1:4 ratio (protein wt:DOPC wt) and dialyzed against 500 volumes of PEN buffer containing 1 mM DTT overnight.[60]

Preparation of Phenylvalerate Micellar Suspension. To prepare phenyl valerate solution, 15 mg of phenylvalerate was dissolved in 1 mL of dimethylformamide (DMF), and 15 mL of water containing 0.03% Triton was added slowly under vigorous stirring.

Formation and Characterization of NEST-Containing tBLMs. Neuropathy target esterase (NTE), an integral membrane protein present in neurons and other cells, including lymphocytes, is the putative target for organophosphorus (OP)-compound-induced delayed neuropathy.[61,62] A segment of NTE that contains the esterase domain (denoted the NEST protein) is commonly used to study the NTE esterase activity.[60,63] NEST esterase activity is generally monitored via its cleavage of the artificial substrate phenylvalerate to form phenol, which can be measured either colorimetrically,[64] in the presence of 4-amino antipyrine, or electrochemically, in the presence of tyrosinase.[65,66]

The inner leaflet of the lipid bilayer was formed as described above. The NEST−DOPC liposome solution was pumped across the inner leaflet at a rate of 0.34 mL/min for 12 min using a syringe pump. Flow was then halted, and adsorption was allowed to continue for approximately 1 h. Five to six flow cell volumes of PEN buffer were then passed through the system to remove the liposomes in the bulk solution. Further details regarding the setup and design of the flow cell can be found in a previous publication.[67]

To measure NEST activity in the tBLM, the PEN buffer in the flow cell was replaced with a micellar suspension of phenyl valerate and allowed to react with the NEST-containing tBLM for 20 min. The resulting suspension was collected, and the amount of phenol produced was measured according to published procedures.[60,64] Briefly, 400 μL of resulting suspension was mixed with 400 μL of 1.23 mM 4-aminoantipyrine containing 3.8 mg of sodium dodecyl sulfate and allowed to react for 5 min. To develop color, 200 μL of 12.1 mM potassium ferricyanide solution was then added to this solution, and after 5 min the absorbance (A) at 486 nm was measured. The spectrophotometer was blanked using suspension obtained in the same way, except the phenyl valerate suspension was treated with a tBLM containing no NEST protein. The amount of phenol produced was determined from the absorbance using a calibration plot depicting A_{486} as a function of known phenol concentrations.

Arrays of Lipid Bilayers. To obtain arrays of tBLMs, a gold-patterned glass slide was dipped in a 1 mM solution of PEG−silane 2000 in absolute ethanol for 20 min, rinsed with absolute ethanol, and heated at 120 °C for 2 h to bind PEG−silane to the exposed glass background of the array. The bottom leaflet of the tBLM was deposited on the gold features as described above. The top leaflet was then added by dipping the modified slide in liposome solution for 45 min and washing with 0.1 M NaCl solution. Because the PEG-background region resisted liposome adsorption, liposomes adsorbed only on the modified gold patterned region.

Electrochemical Impedance Spectroscopy (EIS) Measurements. Impedance measurements were done using an electrochemical analyzer (CH 650A, CH Instruments, Austin, TX). The impedance spectrum was obtained by sweeping an applied potential of 50 mV from 10^{-1} Hz to 10^4 Hz, superimposed on a DC offset of 0 V. A three-electrode configuration was used with a Ag/AgCl reference electrode, a platinum counter electrode, and a modified gold working electrode having an area of 0.16 cm^2. Commercially available software (Z-view, Scribner Associates, Southern Pines, NC) was used to fit electrical circuit models to the impedance spectra.

Fluorescence Recovery after Pattern Photobleaching (FRAPP). FRAPP was used to measure the diffusion coefficients of fluorescently tagged lipid molecules in the tBLM. A system of optical flats[67] was used to toggle between a low-intensity monitoring beam for observation of surface fluorescence and a high intensity beam for photobleaching fluorophores. Liposomes were adsorbed on the electrolessly deposited gold substrates by causing the liposome solution to flow over them at a rate of 0.34 mL/min for 10−12 min using a syringe pump. The infusion was then halted, and liposome adsorption was allowed to continue for approximately 1 h. The flow cell[67] was subsequently flushed with four to five flow cell volumes of 0.1 M NaCl to remove the remaining liposomes in the bulk solution.

FRAPP experiments were conducted in the flow cell by directing the laser beam through a 5× beam expander (Edmund Optics Inc., Barrington, NJ), a filter cube (Ex, 450−490; DM, 510; Em, 515−565), and a Ronchi ruling (50 lines per inch, Edmund Optics Inc., Barrington, NJ), which was placed in the back image plane. The resulting stripe periodicity in the sample plane was 12.5 μm. An aperture was placed in the image plane in front of the photomultiplier tube to reduce the observation area to a size smaller than the photobleached area. This was done to ensure that only fluorescence recovery from the unbleached stripes was monitored (rather than recovery from unbleached areas outside the fringe pattern). The bleaching-beam pulses had an intensity of 0.3−0.5 W and a duration of 0.3−1 s. The monitoring beam had an intensity of 1−3 μW. All experiments were done at room temperature (22 ± 1 °C), which is above the phase transition temperature of DPGP and DOPC[68]

Other Measurements. All fluorescence images were obtained with a Nikon Eclipse E 400 microscope (Nikon, Melville, NY) using a filter cube (Ex, 465−495; DM, 505; Em, 515−555). Field-emission scanning electron microscopy (FE-SEM) images and energy dispersive spectroscopy (EDS) images were obtained using a JEOL 6400 V scanning electron microscope (JEOL USA, Inc., Peabody, MA) equipped with a Noran EDXS detector. Atomic force microscopy (AFM) images were

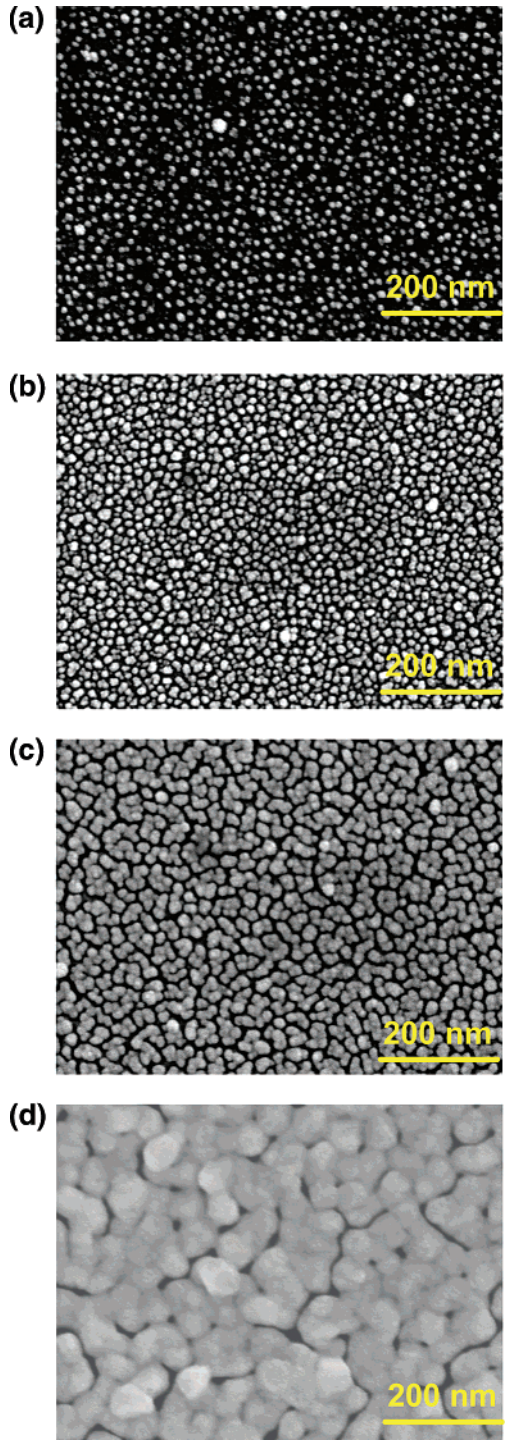

Figure 4. FE-SEM images showing the growth of gold on glass slides: (a) after dipping in colloidal solution, (b) after seeding once, (c) after seeding twice, and (d) after seeding three times.

obtained with a Nanoscope IV multimode scope (Digital Instruments, Santa Barbara, CA) using etched silicon probes in tapping mode. The thickness of the patterned arrays was determined using cross-sectional analysis of the AFM images.

Results and Discussion

Formation of Gold Films. Figure 4a shows a FE-SEM image of a monolayer of gold nanoparticles on a glass slide. The particles were initially not closely packed, so the interface was not conductive. Grabar et al. studied adsorption of gold particles on MPS-coated glass slides and concluded that the particle

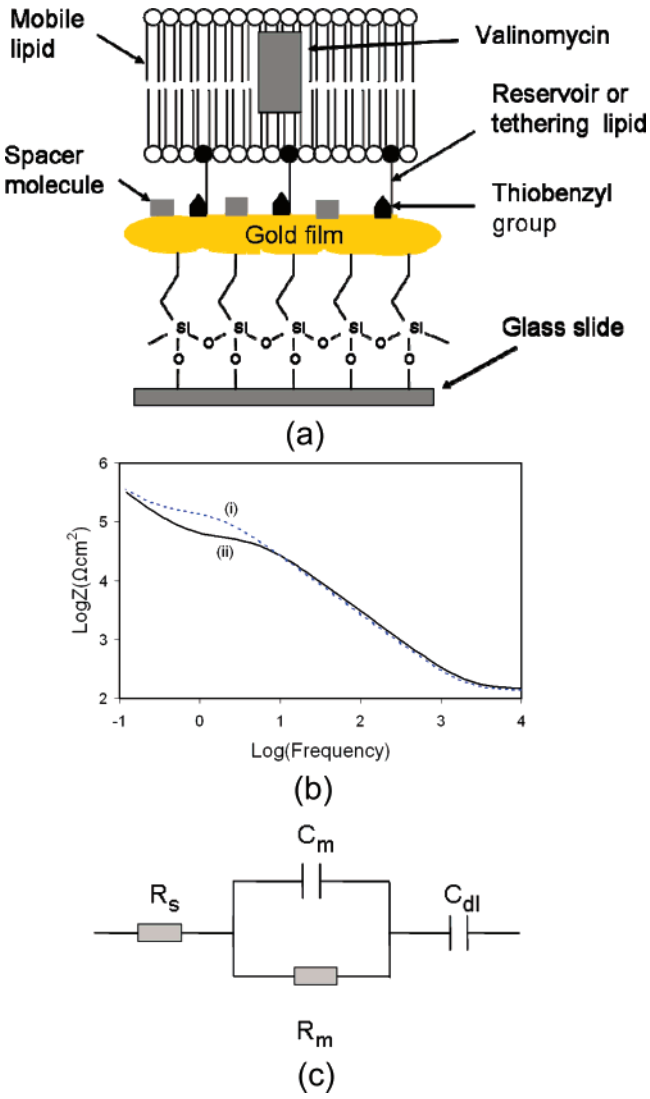

Figure 5. (a) Schematic representation of a tBLM containing an ionophore (valinomycin). (b) Electrochemical spectra of tBLM in a 50 mM KCl/50 mM aqueous NaCl solution before addition of valinomycin (curve i) and after addition of valinomycin (curve ii). (c) Equivalent circuit of a tBLM.

coverage is controlled initially by diffusion and at later times by interparticle repulsion.[69] Colloidal gold particles derived from $[AuCl_4]^-$ have a negative charge resulting from strongly adsorbed Cl^- and/or $[AuCl_2]^-$ produced by incomplete reduction of $[AuCl_4]^-$. This interparticle repulsion prevents the close packing of colloidal gold on the surface.

However, the gold coverage was increased by the seeding step, as shown in Figures 2 and 4b−d. The rate of Au^{3+} reduction on the immobilized gold particles greatly exceeds that in the seeding solution; thus, little new nucleation occurs in the solution, and virtually all of the reduced Au is used to grow the gold particles.[58] The FE-SEM images in Figure 4b−d show the growth of gold film on a glass slide following each successive seeding step. The final gold film had a root-mean-square (rms) roughness of around 10 nm (data not shown). For comparison, a smooth glass slide, a frosted glass slide, and a gold-sputtered silicon wafer have rms roughnesses of about 0.6, 14, and 4 nm, respectively.[26,70]

Functional tBLMs Containing Valinomycin. Figure 5a depicts the spatial organization of the molecules that make up the tBLM. The mobile lipid, DPGP (Figure 1a) forms the bulk of the BLM. The hydrophilic portion of the reservoir lipid DGP

(Figure 1b) establishes the ionic reservoir between the BLM and the gold surface. The hydrophobic portion of the reservoir lipid embeds in the BLM, tethering it to the gold surface. The bulky thiobenzyl moiety of the tethering lipids not only binds the lipid to the gold but also increases the lateral spacing between adjacent reservoir lipid molecules. Cystamine competes with the thiobenzyl group for surface binding sites on the gold and thus it provides a means to further control the spacing between the reservoir lipids.

Figure 5b (curves i and ii) shows Bode plots of tBLM in the absence and presence of valinomycin, respectively, in aqueous solution containing 50 mM KCl/50 mM NaCl. BLMs provide an excellent barrier to ions. Introduction of the K^+-selective ionophore valinomycin into BLM imparts a valinomycin-mediated transmembrane K^+ flux, making it possible to confirm the functionality of valinomycin-containing BLM by measuring differential impedance to potassium and sodium ions.

Figure 5c depicts the electrical analogue model generally used to describe tBLM systems. In this model, the membrane capacitance (C_m) is bypassed by a variable ohmic resistance (R_m), which represents the ionophore-mediated ion flux and any background ion leakage. The membrane capacitance is in series with an effective interfacial capacitance, C_{dl}, which includes the Helmholtz and diffuse capacitances. The model parameters calculated by Z-view software to fit the data in Figure 5b (curve ii) were $C_m = 0.59\ \mu F/cm^2$, $C_{dl} = 3.9\ \mu F/cm^2$, and $R_m = 46\ K\Omega\ cm^2$.

The C_{dl} value in the assembled bilayer system was found to be smaller than the published interfacial capacitance of a gold surface ($\sim 20-30\ \mu F/cm^2$), possibly because of the presence of thiobenzyl groups and cystamine molecules partially blocking the surface or because the tether organizes the water in the reservoir region such that the dielectric constant within the reservoir region is lower than that of the bulk aqueous solution.[28] The value of C_m ($0.59\ \mu F/cm^2$) compared well with the values generally reported for BLM ($\sim 0.5\ \mu F/cm^2$). Additional evidence for the formation of a functional BLM on electrolessly deposited gold films is provided by the decrease in R_m upon the insertion of valinomycin (Figure 5b, curve ii), as indicated by the change in slope at around 10 Hz instead of at around 5 Hz (Figure 5b, curve i) for a lipid bilayer containing no ion channel. The impedance increased again (data not shown) when the aqueous solution (50 mM KCl/50 mM NaCl) was replaced with a solution (100 mM NaCl) containing no KCl. These results provide strong evidence that the valinomycin is embedded in an active conformation in an intact tBLM.

Functional BLM Containing NEST Protein. The phenyl valerate assay was used to confirm whether tBLMs could immobilize NEST in a functional conformation. Incubation of phenyl valerate with NEST-containing BLMs on gold resulted in the production of about 2 ± 0.19 nmol/min of phenol over an area of 1 cm^2. Incubation of phenyl valerate with NEST−DOPC liposomes in solution resulted in the production of 40 ± 1.2 nmol/min of phenol per μg of NEST protein. This result suggests the immobilization of approximately 50 ng/cm^2 of active NEST in tBLMs. To our knowledge, this is the first time NEST has been immobilized in an active conformation on a surface.

BLM Fluidity Measurement Using FRAPP. Figure 6 shows the fluorescence recovery curve for a DGP−DPGP−cystamine modified gold slide contacted with fluorescently labeled liposome solution. Fluorescence recovery was adequately described by a single mobile species model, which assumes only one population of diffusive fluorophores in addition to an immobile fraction. The equation describing pattern photobleaching recovery in such a system is[71,72]

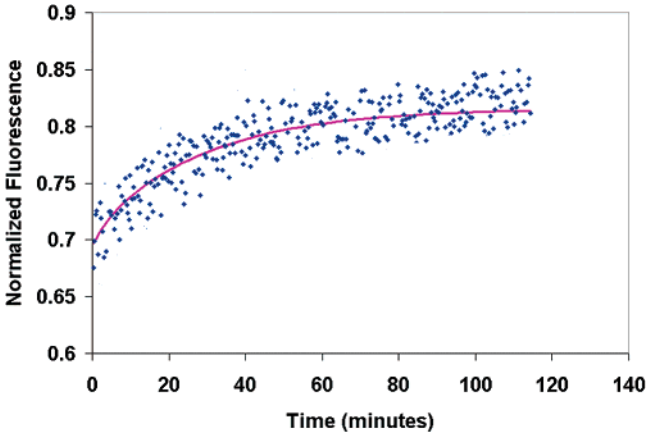

Figure 6. Fluorescence recovery after pattern photobleaching (FRAPP) profile of lipid bilayers on electrolessly deposited gold films. The dots represent postbleach fluorescence intensity normalized against the corresponding prebleach fluorescence value. The solid line represents the fit of eq 1 to the recovery data.

$$f(t) = f(0) + \frac{m}{2}[1 - f(0)]\left[1 - \left(\frac{8}{\pi^2}\right)\left\{\exp\left(-\frac{4\pi^2 Dt}{a^2}\right) + \frac{1}{9}\exp\left(-\frac{36\pi^2 Dt}{a^2}\right)\right\}\right] \quad (1)$$

where $f(t)$ is the ratio of the postbleach fluorescence ($t > 0$) to the prebleach fluorescence, m is the fraction of the fluorophores that are mobile and have a diffusion coefficient D, and a is the stripe periodicity in the sample plane. Unlike spot photobleaching, where 100% recovery is possible for a completely formed sBLM, only 50% recovery is theoretically possible in FRAPP for the same case. Equation 1 was fitted to the FRAPP data, and average best-fit values of D [$(0.12 \pm 0.055) \times 10^{-8}$ cm^2/s] and m (0.87 ± 0.096) were obtained. These values compare well with published values for tBLM.[24]

These results provide strong evidence that the preponderance of the surface is covered by a tBLM. If the surface were covered primarily by unruptured liposomes, extremely low D and m values would be expected, because fluorescently tagged lipids would not transfer freely between adjacent liposomes.

Fabrication and Characterization of Gold Patterns. Parts a and b of Figure 7 show circular and line patterns in gold, respectively, on a glass slide. The lighter features show regions that were in contact with the stamp and are thus covered with gold. The well-defined features of the patterns and the clean background suggest negligible adsorption of gold particles on the background glass slide.

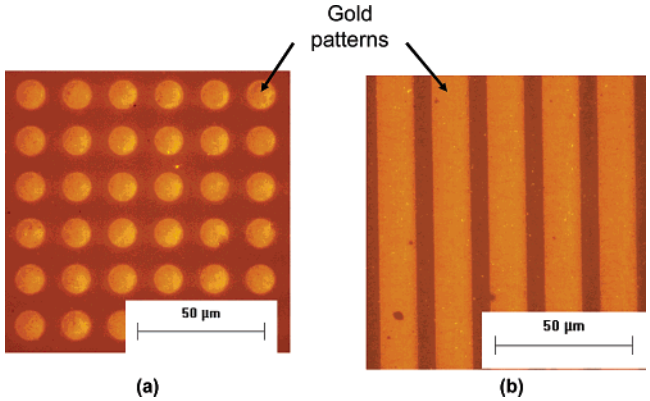

Figure 7. Optical microscopy images of electrolessly deposited gold patterns: (a) circular patterns on a glass slide and (b) line patterns on a glass slide.

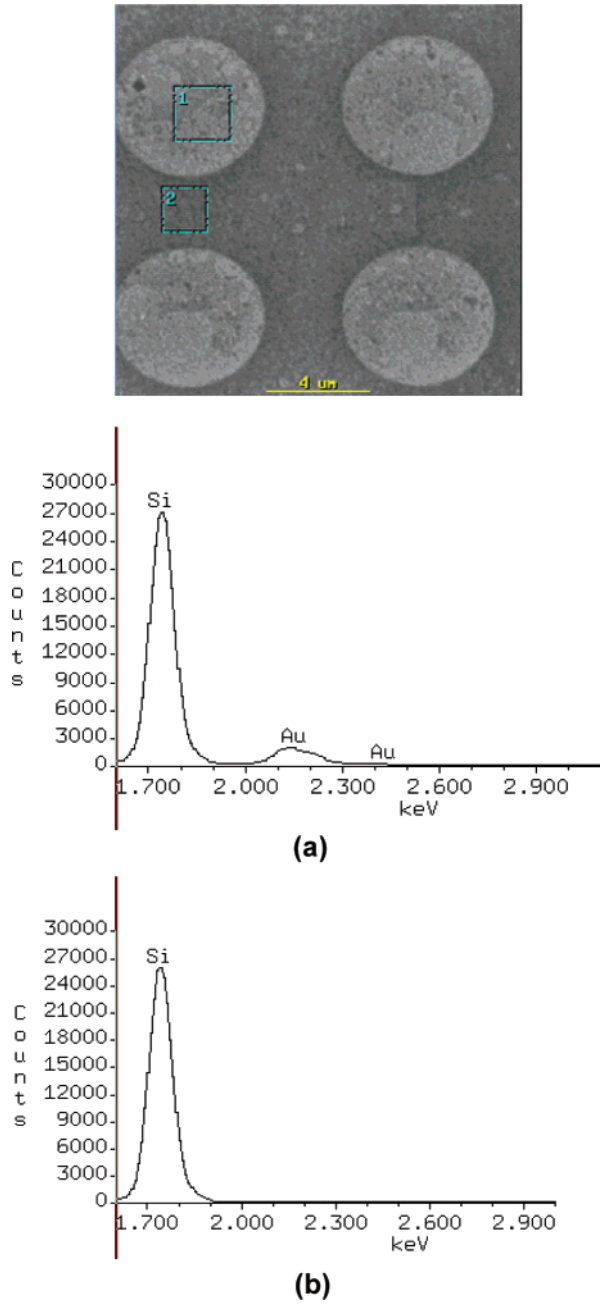

Figure 8. EDS image showing (a) X-rays collected from region 1 (circular patterns) of a SEM image and (b) X-rays collected from region 2 (background) of a SEM image. There is a peak corresponding to Au in X-rays collected from region 1 but not in X-rays from region 2, confirming the selective deposition of Au on the patterned surface.

EDS was also used to confirm selective gold deposition on the patterned regions. In this technique, the area of interest is bombarded with an electron beam of high energy (~10 keV), causing release of X-rays, the wavelengths of which are characteristic of the elements in that region. Figure 8a,b shows that region 1 (MPS patterned region) has a gold peak, but region 2 (background glass slide) does not. These results confirm that gold particles adsorb selectively on the MPS-patterned region. Because the penetration depth of the electron beam is around 10 μm, X-rays from the underlying glass substrate are also collected by the detector. A peak related to Si can also be seen in both figures. Peaks due to other elements generally present in the glass, such as O, Ca, and Al, are not observed, because X-rays associated with these elements lie outside the energy range shown.

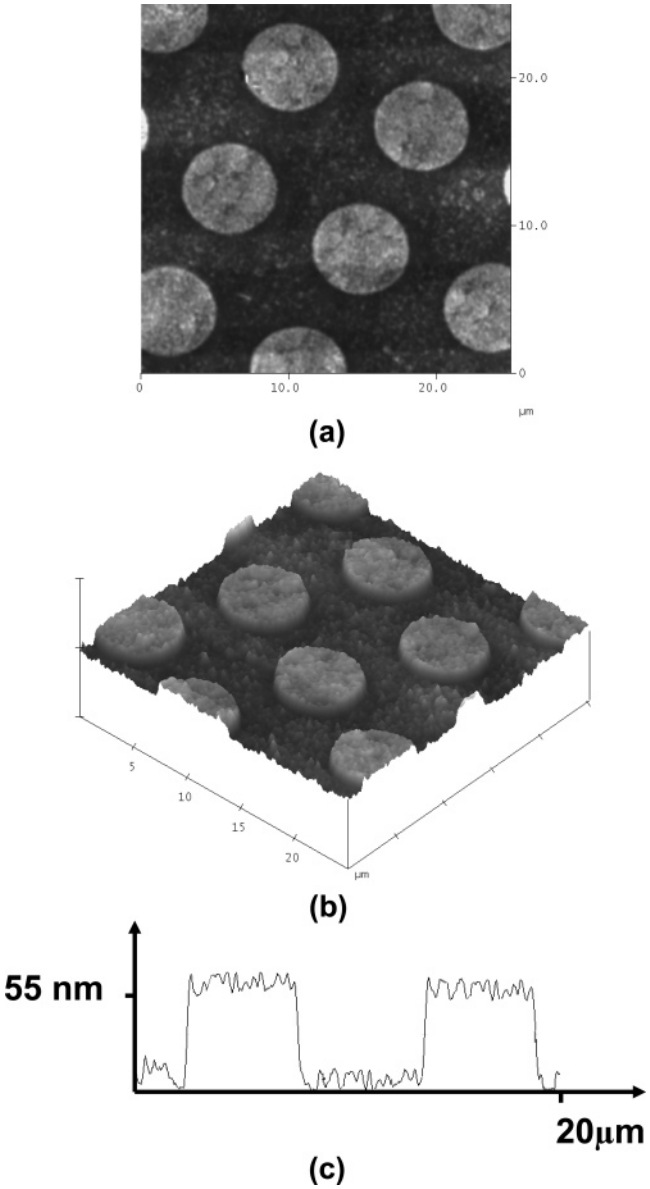

Figure 9. (a) Topographical AFM image of gold patterns on a glass slide, (b) 3-D image of the patterns, and (c) pattern height. All images were obtained in air using tapping mode.

Figure 9a shows an AFM image of gold patterns. The light areas are deposited gold regions, while dark areas are the underlying substrate. Figure 9, parts b and c, shows the 3-D image and topographical image, respectively, of the resulting patterns. The gold regions had an average height of 55 $\pm$ 7 nm and average rms roughness of 10 nm.

Fabrication of tBLM Arrays. PEG coatings have been shown to resist the adsorption of cells as well as macromolecules, such as proteins and polyelectrolytes, through a mechanism that is believed to stem either from steric exclusions between the biomolecule and the PEG chain[73] or from long-range electrostatic repulsions.[74]

Figure 10 shows the fluorescence image of tBLM line patterns. The sharp contrast and clean boundaries between the fluorescent line features and the nonfluorescent background regions, as expected, indicate that fluorescent liposomes bound strongly to the tethering layer (gold patterned region) but not the PEG-coated background region.

While the above-mentioned studies were done on electrolessly deposited gold films on a glass slide, we were also successful

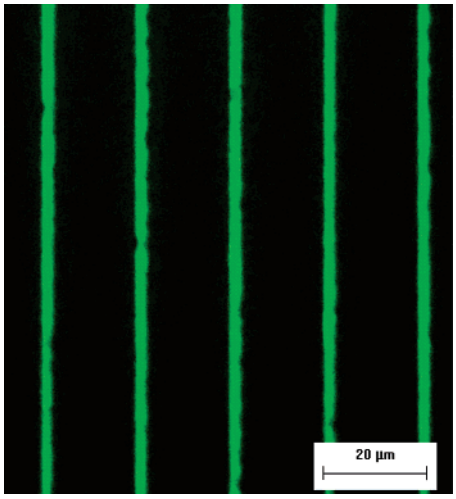

Figure 10. Fluorescence image showing tBLM line patterns in which NBD-PE was the fluorophore.

in forming electrolessly deposited gold films on mechanically flexible substrates, such as plastics, using negatively charged polyelectrolytes and amine-terminated positively charged polyelectrolytes (data not shown).

Significance of Results and Potential Applications. Collectively, the results of this study represent an important milestone toward development of products and processes based on the activities of membrane proteins or other biomolecules. The FE-SEM, EDS, and AFM studies confirmed electroless deposition of gold on an inexpensive substrate (e.g., glass) and showed that the thickness of the gold layer can be controlled. The FRAPP and EIS results showed that silanization, electroless gold deposition, and molecular self-assembly of lipids can be combined to form tBLM on the electrolessly deposited gold. The results with valinomycin and NEST indicated that an ionophore and a fragment of a membrane protein can be bound to the tBLM in an active conformation, so that the activities of these biomolecules can be expressed and measured. The array results indicated that discrete units of the tBLM can be deposited as a high-density microarray that could potentially be used for high-throughput studies of membrane protein or ionophore function. Ongoing research involves applying the interface described here in devices to characterize the functional properties of membrane proteins and cellular interactions with membrane proteins, drug screening, biosensors, biocatalytic reactors, and biological fuel cells.

Conclusions

A versatile approach has been developed that can easily be extended to fabricate functional and nanostructured biomimetic interfaces on a wide variety of surfaces. The approach entails sequentially depositing onto the surface a silane layer, a conductive gold layer, a hydrophilic reservoir, and a tBLM. The diffusion coefficient of the tBLMs on electrolessly deposited gold was comparable to that on vapor-deposited gold. Two different classes of membrane biomolecules, the ionophore valinomycin and the esterase NEST, exhibited their activities when embedded in the tBLM, indicating that the interface can incorporate membrane biomolecules in an active conformation. Because the approach deposits both a conductive gold electrode and a tBLM in close proximity, it can be used for bioelectronic applications, in which the biomolecule's activity is coupled to an electrical signal. Such applications include devices to characterize the functional properties of membrane proteins, biosensors, biocatalytic reactors, and biological fuel cells. Because the entire interface can be fabricated using layer-by-layer assembly from different solutions, this approach may allow biomimetic interfaces to be assembled inside microfluidic channels, thus enabling the production of high-density biosensor arrays for high-throughput applications.

Acknowledgment. This work was funded by the National Science Foundation (CTS No. 0609164), the Michigan Economic Development Corporation's Michigan Technology Tri-Corridor Program, the Center for Fundamental Materials Research, the MSU Intramural Research Grant Program, the MSU Foundation, and the U.S. Army Research Laboratory and U.S. Army Research Office under grant number DAAD19-02-1-0388. The authors thank Dr. P. Glynn for supplying the initial plasmid for the production of NEST.

References and Notes

(1) Ariga, K.; Okahata, Y. *J. Am. Chem. Soc.* **1989**, *111*, 5618−5622.
(2) Fare, T. L. *Langmuir* **1990**, *6*, 1172−1179.
(3) Heyse, S.; Vogel, H.; Sanger, M.; Sigrist, H. *Protein Sci.* **1995**, *4*, 2532−2544.
(4) McConnell, H. M.; Watts, T. H.; Weis, R. M.; Brian, A. A. *Biochim. Biophys. Acta* **1986**, *864*, 95−106.
(5) Nikolelis, D. P.; Siontorou, C. G.; Krull, U. J.; Katrivanos, P. L. *Anal. Chem.* **1996**, *68*, 1735−1741.
(6) Plant, A. L. *Langmuir* **1993**, *9*, 2764−2767.
(7) Plant, A. L.; Gueguetchkeri, M.; Yap, W. *Biophys. J.* **1994**, *67*, 1126−1133.
(8) Seifert, K.; Fendler, K.; Bamberg, E. *Biophys. J.* **1993**, *64*, 384−391.
(9) Stelzle, M.; Sackmann, E. *Biochim. Biophys. Acta* **1989**, *981*, 135−142.
(10) Stenger, D. A.; Fare, T. L.; Cribbs, D. H.; Rustin, K. M. *Biosens. Bioelectron.* **1992**, *7*, 11−20.
(11) Favero, G.; D'Annibale, A.; Campanella, L.; Santucci, R.; Ferri, T. *Anal. Chim. Acta* **2002**, *460*, 23−34.
(12) Furuike, S.; Hirokawa, J.; Yamada, S.; Yamazaki, M. *Biochim. Biophys. Acta-Biomembr.* **2003**, *1615*, 1−6.
(13) Glasmastar, K.; Larsson, C.; Hook, F.; Kasemo, B. *J. Colloid Interface Sci.* **2002**, *246*, 40−47.
(14) Graneli, A.; Rydstrom, J.; Kasemo, B.; Hook, F. *Langmuir* **2003**, *19*, 842−850.
(15) Groves, J. T.; Mahal, L. K.; Bertozzi, C. R. *Langmuir* **2001**, *17*, 5129−5133.
(16) Lahiri, J.; Kalal, P.; Frutos, A. G.; Jonas, S. T.; Schaeffler, R. *Langmuir* **2000**, *16*, 7805−7810.
(17) Ohlsson, P. A.; Tjarnhage, T.; Herbai, E.; Lofas, S.; Puu, G. *Bioelectrochem. Bioenerg.* **1995**, *38*, 137−148.
(18) Tien, H. T.; Barish, R. H.; Gu, L. Q.; Ottova, A. L. *Anal. Sci.* **1998**, *14*, 3−18.
(19) Tien, H. T.; Ottova, A. L. *Electrochim. Acta* **1998**, *43*, 3587−3610.
(20) Hoppe, W.; Lohmann, W. *Biophysics*; Springer-Verlag: Berlin, 1983.
(21) Heibel, C.; Maus, S.; Knoll, W.; Ruhe, J. In *Organic Thin Films*; American Chemical Society: Washington, DC, 1998; Vol. 695, pp 104−118.
(22) Krishna, G.; Schulte, J.; Cornell, B. A.; Pace, R.; Wieczorek, L.; Osman, P. D. *Langmuir* **2001**, *17*, 4858−4866.
(23) Moncelli, M. R.; Becucci, L.; Schiller, S. M. *Bioelectrochemistry* **2004**, *63*, 161−167.
(24) Munro, J. C.; Frank, C. W. *Langmuir* **2004**, *20*, 3339−3349.
(25) Naumann, C. A.; Prucker, O.; Lehmann, T.; Ruhe, J.; Knoll, W.; Frank, C. W. *Biomacromolecules* **2002**, *3*, 27−35.
(26) Naumann, R.; Schiller, S. M.; Giess, F.; Grohe, B.; Hartman, K. B.; Karcher, I.; Koper, I.; Lubben, J.; Vasilev, K.; Knoll, W. *Langmuir* **2003**, *19*, 5435−5443.
(27) Naumann, R.; Walz, D.; Schiller, S. M.; Knoll, W. *J. Electroanal. Chem.* **2003**, *550*, 241−252.
(28) Raguse, B.; Braach-Maksvytis, V.; Cornell, B. A.; King, L. G.; Osman, P. D. J.; Pace, R. J.; Wieczorek, L. *Langmuir* **1998**, *14*, 648−659.
(29) Shen, W. W.; Boxer, S. G.; Knoll, W.; Frank, C. W. *Biomacromolecules* **2001**, *2*, 70−79.

(30) Sinner, E. K.; Knoll, W. *Curr. Opin. Chem. Biol.* **2001**, *5*, 705−711.
(31) Tanaka, S.; Iwasaki, Y.; Ishihara, K.; Nakabayashi, N. *Macromol. Rapid Commun.* **1994**, *15*, 319−326.
(32) Theato, P.; Zentel, R. *Langmuir* **2000**, *16*, 1801−1805.
(33) Zhang, L. Q.; Longo, M. L.; Stroeve, P. *Langmuir* **2000**, *16*, 5093−5099.
(34) Kumar, A.; Whitesides, G. M. *Appl. Phys. Lett.* **1993**, *63*, 2002−2004.
(35) Kohli, N.; Dvornic, P.; Kaganove, S.; Worden, M.; Lee, I. *Macromol. Rapid Commun.* **2004**, *25*, 935−941.
(36) St. John, P. M.; Craighead, H. G. *Appl. Phys. Lett.* **1996**, *68*, 1022−1024.
(37) Xia, Y.; Kim, E.; Mrksich, M.; Whitesides, G. M. *Chem. Mater.* **1996**, *8*, 601−603.
(38) Yang, X. M.; Tryk, D. A.; Hasimoto, K.; Fujishima, A. *Appl. Phys. Lett.* **1996**, *69*, 4020−4022.
(39) Kohli, N.; Worden, R. M.; Lee, I. *Chem. Commun.* **2005**, *3*, 316−318.
(40) Berg, M. C.; Yang, S. Y.; Hammond, P. T.; Rubner, M. F. *Langmuir* **2004**, *20*, 1362−1368.
(41) Kim, H.; Doh, J.; Irvine, D. J.; Cohen, R. E.; Hammond, P. T. *Biomacromolecules* **2004**, *5*, 822−827.
(42) Yang, S. Y.; Mendelsohn, J. D.; Rubner, M. F. *Biomacromolecules* **2003**, *4*, 987−994.
(43) Groves, J. T.; Boxer, S. G. *Acc. Chem. Res.* **2002**, *35*, 149−157.
(44) Groves, J. T.; Ulman, N.; Boxer, S. G. *Science* **1997**, *275*, 651−653.
(45) Hovis, J. S.; Boxer, S. G. *Langmuir* **2000**, *16*, 894−897.
(46) Kung, L. A.; Kam, L.; Hovis, J. S.; Boxer, S. G. *Langmuir* **2000**, *16*, 6773−6776.
(47) Bittner, A. M.; Wu, X. C.; Kern, K. *Adv. Funct. Mater.* **2002**, *12*, 432−436.
(48) Delamarche, E.; Vichiconti, J.; Hall, S. A.; Geissler, M.; Graham, W.; Michel, B.; Nunes, R. *Langmuir* **2003**, *19*, 6567−6569.
(49) Geissler, M.; Kind, H.; Schmidt-Winkel, P.; Michel, B.; Delamarche, E. *Langmuir* **2003**, *19*, 6283−6296.
(50) Guo, T. F.; Chang, S. C.; Pyo, S.; Yang, Y. *Langmuir* **2002**, *18*, 8142−8147.
(51) Hidber, P. C.; Helbig, W.; Kim, E.; Whitesides, G. M. *Langmuir* **1996**, *12*, 1375−1380.
(52) Hidber, P. C.; Nealey, P. F.; Helbig, W.; Whitesides, G. M. *Langmuir* **1996**, *12*, 5209−5215.
(53) Moran, C. E.; Radloff, C.; Halas, N. J. *Adv. Mater.* **2003**, *15*, 804.
(54) Ng, W. K.; Wu, L.; Moran, P. M. *Appl. Phys. Lett.* **2002**, *81*, 3097−3099.
(55) Wu, X. C.; Bittner, A. M.; Kern, K. *Langmuir* **2002**, *18*, 4984−4988.
(56) Wu, X. C.; Bittner, A. M.; Kern, K. *Adv. Mater.* **2004**, *16*, 413−+.
(57) Guan, F.; Chen, M. A.; Yang, W.; Wang, J. Q.; Yong, S. R.; Xue, Q. J. *Appl. Surf. Sci.* **2005**, *240*, 24−27.
(58) Supriya, L.; Claus, R. O. *Langmuir* **2004**, *20*, 8870−8876.
(59) Frens, G. *Nat.-Phys. Sci.* **1973**, *241*, 20−22.
(60) Atkins, J.; Glynn, P. *J. Biol. Chem.* **2000**, *275*, 24477−24483.
(61) Glynn, P. *Biochem. J.* **1999**, *344*, 625−631.
(62) Makhaeva, G. F.; Sigolaeva, L. V.; Zhuravleva, L. V.; Eremenko, A. V.; Kurochkin, I. N.; Malygin, V. V.; Richardson, R. J. *J. Toxicol. Environ. Health-Part A* **2003**, *66*, 599−610.
(63) Kropp, T. J.; Glynn, P.; Richardson, R. J. *Biochemistry* **2004**, *43*, 3716−3722.
(64) Kayyali, U. S.; Moore, T. B.; Randall, J. C.; Richardson, R. J. *J. Anal. Toxicol.* **1991**, *15*, 86−89.
(65) Sigolaeva, L. V.; Makower, A.; Eremenko, A. V.; Makhaeva, G. F.; Malygin, V. V.; Kurochkin, I. N.; Scheller, F. W. *Anal. Biochem.* **2001**, *290*, 1−9.
(66) Sokolovskaya, L. G.; Sigolaeva, L. V.; Eremenko, A. V.; Gachok, I. V.; Makhaeva, G. F.; Strakhova, N. N.; Malygin, V. V.; Richardson, R. J.; Kurochkin, I. N. *Biotechnol. Lett.* **2005**, *27*, 1211−1218.
(67) Gajraj, A.; Ofoli, R. Y. *Langmuir* **2000**, *16*, 4279−4285.
(68) In *Lipid-Protein Interactions*; Silvius, J. R., Ed.; John Wiley & Sons, Inc.: New York, 1982.
(69) Grabar, K. C.; Smith, P. C.; Musick, M. D.; Davis, J. A.; Walter, D. G.; Jackson, M. A.; Guthrie, A. P.; Natan, M. J. *J. Am. Chem. Soc.* **1996**, *118*, 1148−1153.
(70) Tristram-Nagle, S.; Petrache, H. I.; Suter, R. M.; Nagle, J. F. *Biophys. J.* **1998**, *74*, A203−A203.
(71) Wright, L. L.; Palmer, A. G.; Thompson, N. L. *Biophys. J.* **1988**, *54*, 463−470.
(72) Smith, B. A.; McConnell, H. M. *Proc. Natl. Acad. Sci. U.S.A.* **1978**, *75*, 2759−2763.
(73) Harris, J. M. *Poly(ethylene glycol) chemistry: Biotechnical and Biomedical Applications*; Plenum Press: New York, 1992.
(74) Feldman, K.; Hahner, G.; Spencer, N. D.; Harder, P.; Grunze, M. *J. Am. Chem. Soc.* **1999**, *121*, 10134−10141.

BM0603995